17. LATTICE QUANTUM CHROMODYNAMICS

Updated September 2013 by S. Hashimoto (KEK), J. Laiho (Syracuse University), and S.R. Sharpe (University of Washington).

17.1. Lattice regularization of QCD

Gauge theories form the building blocks of the Standard Model. While the SU(2) and U(1) parts have weak couplings and can be studied accurately with perturbative methods, the SU(3) component—QCD—is only amenable to a perturbative treatment at high energies. The growth of the coupling constant in the infrared—the flip-side of asymptotic freedom—requires the use of non-perturbative methods to determine the low energy properties of QCD. Lattice gauge theory, proposed by K. Wilson in 1974 [1], provides such a method, for it gives a non-perturbative definition of vector-like gauge field theories like QCD. In lattice regularized QCD—commonly called lattice QCD or LQCD—Euclidean space-time is discretized, usually on a hypercubic lattice with lattice spacing a, with quark fields placed on sites and gauge fields on the links between sites. The lattice spacing plays the role of the ultraviolet regulator, rendering the quantum field theory finite. The continuum theory is recovered by taking the limit of vanishing lattice spacing, which can be reached by tuning the bare coupling constant to zero according to the renormalization group.

Unlike dimensional regularization, which is commonly used in continuum QCD calculations, the definition of LQCD does not rely on the perturbative expansion. Indeed, LQCD allows non-perturbative calculations by numerical evaluation of the path integral that defines the theory.

Practical LQCD calculations are limited by the availability of computational resources and the efficiency of algorithms. Because of this, LQCD results come with both statistical and systematic errors, the former arising from the use of Monte-Carlo integration, the latter, for example, from the use of non-zero values of a. There are also different ways in which the QCD action can be discretized, and all must give consistent results in the continuum limit, $a \to 0$. It is the purpose of this review to provide an outline of the methods of LQCD, with particular focus on applications to particle physics, and an overview of the various sources of error. This should allow the reader to better understand the LQCD results that are presented in other sections for a variety of quantities (quark masses, the hadron spectrum and several electroweak matrix elements). For more extensive explanations the reader should consult the available textbooks or lecture notes, the most up-to-date of which are Refs. [2–4].

17.1.1. *Gauge invariance, gluon fields and the gluon action* :

A key feature of the lattice formulation of QCD is that it preserves gauge invariance. This is in contrast to perturbative calculations, where gauge fixing is an essential step. The preservation of gauge invariance leads to considerable simplifications, e.g. restricting the form of operators that can mix under renormalization.

The gauge transformations of lattice quark fields are just as in the continuum: $q(x) \longrightarrow V(x)q(x)$ and $\bar{q}(x) \longrightarrow \bar{q}(x)V^\dagger(x)$, with $V(x)$ an arbitrary element of SU(3).

The only difference is that the Euclidean space-time positions x are restricted to lie on the sites of the lattice, i.e. $x = a(n_1, n_2, n_3, n_4)$ for a hypercubic lattice, with the n_j being integers. Quark bilinears involving different lattice points can be made gauge invariant by introducing the gluon field $U_\mu(x)$. For example, for adjacent points the bilinear is $\bar{q}(x)U_\mu(x)q(x+a\hat{\mu})$, with $\hat{\mu}$ the unit vector in the μ'th direction. (This form is used in the construction of the lattice covariant derivative.) The gluon field (or "gauge link") is an element of the group, SU(3), in contrast to the continuum field A_μ which takes values in the Lie algebra. The bilinear is invariant if U_μ transforms as $U_\mu(x) \to V(x)U_\mu(x)V^\dagger(x+a\hat{\mu})$. The lattice gluon field is naturally associated with the link joining x and $x+a\hat{\mu}$, and corresponds in the continuum to a Wilson line connecting these two points, $P \exp(i \int_x^{x+a\hat{\mu}} dx_\mu A_\mu^{\text{cont}}(x))$ (where P indicates a path-ordered integral, and the superscript on A_μ indicates that it is a continuum field). The trace of a product of the $U_\mu(x)$ around any closed loop is easily seen to be gauge invariant and is the lattice version of a Wilson loop.

The simplest possible gauge action, usually called the Wilson gauge action, is given by the product of gauge links around elementary plaquettes:

$$S_g = \beta \sum_{x,\mu,\nu} [1 - \frac{1}{3}\text{ReTr}[U_\mu(x)U_\nu(x+a\hat{\mu})U_\mu^\dagger(x+a\hat{\nu})U_\nu^\dagger(x)]] . \qquad (17.1)$$

For small a, assuming that the fields are slowly varying, one can expand the action in powers of a using $U_\mu(x) = \exp(iaA_\mu(x))$. Keeping only the leading non-vanishing term, and replacing the sum with an integral, one finds the continuum form,

$$S_g \longrightarrow \int d^4x \frac{1}{4g_{\text{lat}}^2}\text{Tr}[F_{\mu\nu}^2(x)] , \qquad (F_{\mu\nu} = \partial_\mu A_\nu - \partial_\nu A_\mu + i[A_\mu, A_\nu]) \qquad (17.2)$$

as long as one chooses $\beta = 6/g_{\text{lat}}^2$ for the lattice coupling. In this expression, g_{lat} is the bare coupling constant in the lattice scheme, which can be related (by combining continuum and lattice perturbation theory) to a more conventional coupling constant such as that in the $\overline{\text{MS}}$ scheme (see Sec. 17.3.4 below).

In practice, the lattice spacing a is non-zero, leading to discretization errors. In particular, the lattice breaks Euclidean rotational invariance (which is the Euclidean version of Lorentz invariance) down to a discrete hypercubic subgroup. One wants to reduce discretization errors as much as possible. A very useful tool for understanding and then reducing discretization errors is the Symanzik effective action: the interactions of quarks and gluons with momenta low compared to the lattice cutoff ($|p| \ll 1/a$) are described by a continuum action consisting of the standard continuum terms (e.g. the gauge action given in Eq. (17.2)) augmented by higher dimensional operators suppressed by powers of a [5]. For the Wilson lattice gauge action, the leading corrections come in at $\mathcal{O}(a^2)$. They take the form $\sum_j a^2 c_j O_6^{(j)}$, with the sum running over all dimension-six operators $O_6^{(j)}$ allowed by the *lattice* symmetries, and c_j unknown coefficients. Some of these operators violate Euclidean invariance, and all of them lead to discretization errors

of the form $a^2\Lambda^2$, where Λ is a typical momentum scale for the quantity being calculated. These errors can, however, be reduced by adding corresponding operators to the lattice action and tuning their coefficients to eliminate the dimension-six operators in the effective action to a given order in perturbation theory or even non-perturbatively. This is the idea of the Symanzik improvement program [5]. In the case of the gauge action, one adds Wilson loops involving six gauge links (as opposed to the four links needed for the original plaquette action, Eq. (17.1)) to define the $\mathcal{O}(a^2)$ improved (or "Symanzik") action [6]. In practical implementations, the improvement is either at tree-level (so that residual errors are proportional to $\alpha_s a^2$, where the coupling is evaluated at a scale $\sim 1/a$), or at one loop order (errors proportional to $\alpha_s^2 a^2$). Another popular choice is motivated by studies of renormalization group (RG) flow. It has the same terms as the $\mathcal{O}(a^2)$ improved action but with different coefficients, and is called the RG-improved or "Iwasaki" action [7].

17.1.2. *Lattice fermions* :

Discretizing the fermion action turns out to involve subtle issues, and the range of actions being used is more extensive than for gauge fields. Recall that the continuum fermion action is $S_f = \int d^4x \bar{q}[iD_\mu\gamma_\mu + m_q]q$, where $D_\mu = \partial_\mu + iA_\mu$ is the gauge-covariant derivative. The simplest discretization replaces the derivative with a symmetric difference:

$$D_\mu q(x) \longrightarrow \frac{1}{2a}[U_\mu(x)q(x+a\hat{\mu}) - U_\mu(x-a\hat{\mu})^\dagger q(x-a\hat{\mu})]. \qquad (17.3)$$

The factors of U_μ ensure that $D_\mu q(x)$ transforms under gauge transformations in the same way as $q(x)$, so that the discretized version of $\bar{q}(x)D_\mu\gamma_\mu q(x)$ is gauge invariant. The choice in Eq. (17.3) leads to the so-called naive fermion action. This, however, suffers from the fermion doubling problem—in d dimensions it describes 2^d equivalent fermion fields in the continuum limit . The appearance of the extra "doubler" fermions is related to the deeper theoretical problem of formulating chirally symmetric fermions on the lattice. This is encapsulated by the Nielsen-Ninomiya theorem [8]: one cannot define lattice fermions having exact, continuum-like chiral symmetry without producing doublers. Naive lattice fermions do have chiral symmetry but at the cost of introducing 15 unwanted doublers (for $d = 4$).

There are a number of different strategies for dealing with the doubling problem, each with their own theoretical and computational advantages and disadvantages. Wilson fermions [1] add a term proportional to $a\bar{q}\Delta q$ to the fermion action (the "Wilson term"—in which Δ is a covariant lattice Laplacian). This gives a mass of $\mathcal{O}(1/a)$ to the doublers, so that they decouple in the continuum limit. The Wilson term, however, violates chiral symmetry, and also introduces discretization errors linear in a. A commonly used variant that eliminates the $\mathcal{O}(a)$ discretization error is the $\mathcal{O}(a)$-improved Wilson (or "clover") fermion [9]. In this application of Symanzik improvement, methods have been developed to remove $\mathcal{O}(a)$ terms non-perturbatively using auxiliary simulations to tune parameters [10]. Such "non-perturbative improvement" is of great practical importance as it brings the discretization error from the fermion action down to the same level as that from the gauge action. It is used by essentially all simulations using clover fermions.

The advantages of Wilson fermions are their theoretical simplicity and relatively low computational cost. Their main disadvantage is the lack of chiral symmetry, which makes them difficult to use in cases where mixing with wrong chirality operators can occur, particularly if this involves divergences proportional to powers of $1/a$. A related problem is the presence of potential numerical instabilities due to spurious near-zero modes of the lattice Dirac operator. Ongoing work has, however, been successful at ameliorating these problems and increasing the range of quantities for which Wilson fermions can be used [11,12].

Twisted-mass fermions [13] are a variant of Wilson fermions in which two flavors are treated together with an isospin-breaking mass term (the "twisted mass" term). The main advantage of this approach is that all errors linear in a are automatically removed (without the need for tuning of parameters) by a clever choice of twisted mass and operators [14]. A disadvantage is the presence of isospin breaking effects (such as a splitting between charged and neutral pion masses even when up and down quarks are degenerate), which, however, vanish as $a^2\Lambda^2$ in the continuum limit.

Staggered fermions are a reduced version of naive fermions in which there is only a single fermion Dirac component on each lattice site, with the full Dirac structure built up from neighboring sites [15]. They have the advantages of being somewhat faster to simulate than Wilson-like fermions, of preserving some chiral symmetry, and of having discretization errors of $\mathcal{O}(a^2)$. Their disadvantage is that they retain some of the doublers (3 for $d = 4$). The action thus describes four degenerate fermions in the continuum limit. These are usually called "tastes", to distinguish them from physical flavors, and the corresponding SU(4) symmetry is referred to as the "taste symmetry". The preserved chiral symmetry in this formulation has non-singlet taste. Practical applications usually introduce one staggered fermion for each physical flavor, and remove contributions from the unwanted tastes by taking the fourth-root of the fermion determinant appearing in the path integral. The validity of this "rooting" procedure is not obvious because taste symmetry is violated for non-zero lattice spacing. Theoretical arguments, supported by numerical evidence, suggest that the procedure is valid as long as one takes the continuum limit before approaching the light quark mass region [16]. Additional issues arise for the valence quarks (those appearing in quark propagators, as described in Sec. 17.2 below), where rooting is not possible, and one must remove the extra tastes by hand [17].

Just as for Wilson fermions, the staggered action can be improved, so as to reduce discretization errors. The widely used "asqtad" action [18] removes tree-level $\mathcal{O}(a^2)$ errors, and leads to substantial reduction in the breaking of taste symmetry. More recently, a highly improved staggered quark ("HISQ") action has been introduced [19], which further reduces discretization errors, both those which break taste symmetry and those which do not. It is tuned to reduce discretization errors for both light and heavier quarks, and is being used to directly simulate charm quarks.

There is an important class of lattice fermions, "Ginsparg-Wilsons fermions", that possess a continuum-like chiral symmetry without introducing unwanted doublers. The lattice Dirac operator D for these fermions satisfies the Ginsparg-Wilson relation $D\gamma_5 + \gamma_5 D = aD\gamma_5 D$ [20]. In the continuum, the right-hand-side vanishes due to chiral symmetry. On the lattice, it is non-vanishing, but with a particular form (with two

factors of D) that restricts the violations of chiral symmetry in Ward-Takahashi identities to short-distance terms that do not contribute to physical matrix elements [21]. In fact, one can define a modified chiral transformation on the lattice (by including dependence on the gauge fields) such that Ginsparg-Wilson fermions have an exact chiral symmetry for on-shell quantities [22]. The net result is that such fermions essentially have the same properties under chiral transformations as do continuum fermions, including the index theorem [21]. Their leading discretization errors are of $\mathcal{O}(a^2)$.

Two types of Ginsparg-Wilson fermions are currently being used in large-scale numerical simulations. The first are Domain-wall fermions (DWF). These are defined on a five-dimensional space, in which the fifth dimension is fictitious [23]. The action is chosen so that the low-lying modes are chiral, with left- and right-handed modes localized on opposite four-dimensional surfaces. For an infinite fifth dimension, these fermions satisfy the Ginsparg-Wilson relation. In practice, the fifth dimension is kept finite, and there remains a small, controllable violation of chiral symmetry. The second type are Overlap fermions. These appeared from a completely different context and have an explicit form that exactly satisfies the Ginsparg-Wilson relation [24]. Their numerical implementation requires an approximation of the matrix sign function of a Wilson-like fermion operator, and various approaches are being used. In fact, it is possible to rewrite these approximations in terms of a five-dimensional formulation, showing that the DWF and Overlap approaches are essentially equivalent [25]. Numerically, the five-dimensional approach appears to be the most computationally efficient.

As noted above, each fermion formulation has its own advantages and disadvantages. For instance, domain-wall and overlap fermions are theoretically preferred as they have chiral symmetry without doublers, but their computational cost is at least an order of magnitude greater than for other choices. If the physics application of interest and the target precision do not require near-exact chiral symmetry, there is no strong motivation to use these expensive formulations. On the other hand, there is a class of applications (including the calculation of the $\Delta I = 1/2$ amplitude for $K \to \pi\pi$ decays and the S-parameter [26]) where chiral symmetry plays an essential role and for which the use of Ginsparg-Wilson fermions is strongly favored.

17.1.3. *Heavy quarks on the lattice* :

The fermion formulations described in the previous subsection can be used straightforwardly only for quarks whose masses are small compared to the lattice cutoff, $m_q \lesssim 1/a$. This is because there are discretization errors proportional to powers of am_q, and if $am_q \gtrsim 1$ these errors are large and uncontrolled. Present LQCD simulations typically have cutoffs in the range of $1/a = 2 - 4$ GeV (corresponding to $a \approx 0.1 - 0.05$ fm). Thus, while for the up, down and strange quarks one has $am_q \ll 1$, for bottom quarks (with $m_b \approx 4.5$ GeV) one must use alternative approaches. Charm quarks ($m_c \approx 1.5$ GeV) are an intermediate case, allowing simulations using both direct and alternative approaches.

For the charm quark, the straightforward approach is to simultaneously reduce the lattice spacing and to improve the fermion action so as to reduce the size of errors proportional to powers of am_c. This approach has, for example, been followed successfully

using the HISQ and twisted-mass actions [19,27,28]. It is important to note, however, that reducing a increases the computational cost because an increased number of lattice points are needed for the same physical volume. One cannot reduce the spatial size below $2 - 3$ fm without introducing finite volume errors. Present lattices have sizes up to $\sim 96^3 \times 192$ (with the long direction being Euclidean time), and thus allow a lattice cutoff up to $1/a \sim 4$ GeV.

Alternative approaches for discretizing heavy quarks are motivated by effective field theories. For a bottom quark in heavy-light hadrons, one can use Heavy Quark Effective Theory (HQET) to expand about the infinite quark-mass limit. In this limit, the bottom quark is a static color source, and one can straightforwardly write the corresponding lattice action [29]. Corrections, proportional to powers of $1/m_b$, can be introduced as operator insertions, with coefficients that can be determined non-perturbatively using existing techniques [30]. This method allows the continuum limit to be taken controlling all $1/m_b$ corrections.

Another way of introducing the $1/m_b$ corrections is to include the relevant terms in the effective action. This leads to a non-relativistic QCD (NRQCD) action, in which the heavy quark is described by a two-component spinor [31]. This approach has the advantage over HQET that it can also be used for heavy-heavy systems, such as the Upsilon states. A disadvantage is that some of the parameters in this effective theory are determined perturbatively (originally at tree-level, but more recently at one-loop), which limits the precision of the final results. Although discretization effects can be controlled with good numerical precision for a range of lattice spacings, at fine enough lattice spacing the NRQCD effective theory no longer applies since power divergent terms become important, and taking the continuum limit would require fine-tuning a large number of couplings non-perturbatively.

This problem can be avoided if one uses HQET power counting to analyze and reduce discretization effects for heavy quarks while using conventional fermion actions [32]. For instance, one can tune the parameters of an improved Wilson quark action so that the leading HQET corrections to the static quark limit are correctly accounted for. As the lattice spacing becomes finer, the action smoothly goes over to that of a light Wilson quark action, where the continuum limit can be taken as usual. In principle, one can improve the action in the heavy quark regime up to arbitrarily high orders using HQET, but so far large-scale simulations have typically used clover improved Wilson quarks, where tuning the parameters of the action corresponds to including all corrections through next-to-leading order in HQET. Three different methods for tuning the parameters of the clover action are being used: the Fermilab [32], Tsukuba [33] and Columbia [34] approaches. An advantage of this HQET approach is that the c and b quarks can be treated on the same footing. Parameter tuning has typically been done perturbatively, as in NRQCD, but recent work using the Columbia approach has used non-perturbative tuning [35].

17.1.4. *Basic inputs for lattice calculations* :

Since LQCD is nothing but a regularization of QCD, the renormalizability of QCD implies that the number of input parameters in LQCD is the same as for continuum QCD—the strong coupling constant $\alpha_s = g^2/(4\pi)$, the quark masses for each flavor, and the CP violating phase θ. The θ parameter is usually assumed to be zero, while the other parameters must be determined using experimental inputs.

17.1.4.1. *Lattice spacing:* In QCD, the coupling constant is a function of scale. With lattice regularization, this scale is the inverse lattice spacing $1/a$, and choosing the bare coupling constant is equivalent to fixing the lattice spacing.

In principle, a can be determined using any dimensionful quantity measured by experiments. For example, using the mass of hadron H one has $a = (am_H)^{\rm lat}/m_H^{\rm exp}$. (Of course, one must first tune the quark masses to their physical values, as discussed below.) In practice, one chooses quantities that can be calculated accurately on the lattice, and that are only weakly dependent on the light quark masses. The latter property minimizes errors from extrapolating or interpolating to the physical light quark masses or from mistuning of these masses. Commonly used choices are the spin-averaged 1S-1P or 1S-2S splittings in the Upsilon system, the mass of the Ω^- baryon, and the pion decay constant f_π. Ultimately, all choices must give the consistent results for a, and that this is the case provides a highly non-trivial check of both the calculational method and of QCD.

The determination of a using quantities involving light (up and down) quarks—such as f_π—involves particular challenges. Most current lattice simulations are done using light quark masses heavier than those in nature. One thus has to extrapolate the lattice data towards the physical quark masses. This "chiral extrapolation" is non-trivial because the quark mass dependence may involve non-analytic terms due to the loops of nearly massless pions, as predicted by Chiral Perturbation Theory (ChPT) [36].

17.1.4.2. *Light quark masses:* In LQCD simulations, the up, down and strange quarks are usually referred to as the light quarks, in the sense that $m_q < \Lambda_{\rm QCD}$. (The standard definition of $\Lambda_{\rm QCD}$ is given in the "Quantum Chromodynamics" review; in this review we are using it only to indicate the approximate non-perturbative scale of QCD.) This condition is stronger than that used above to distinguish quarks with small discretization errors, $m_q < 1/a$. Loop effects from light quarks must be included in the simulations to accurately represent QCD. At present, most simulations are done in the isospin symmetric limit $m_u = m_d \equiv m_\ell$, and are often referred to as "$N_f = 2 + 1$" simulations. (If, in addition, one includes the charm quark, this is denoted as an $N_f = 2 + 1 + 1$ simulation.) Precision is now reaching the point where isospin breaking effects, as well as those of electromagnetism (EM) must be included. This can be done approximately using ChPT and other theoretical input, but ultimately one needs to simulate directly with $m_u \neq m_d$ and including QED corrections. Such work is now beginning.

To tune m_ℓ and m_s to their physical values, the most commonly used quantities are, respectively, m_π and m_K. If the scale is being set by m_Ω, then one adjusts the lattice light quark masses until the ratios m_π/m_Ω and m_K/m_Ω take their physical values. At leading order in ChPT, one has the Gell-Mann-Oakes-Renner relations $m_{\pi^0}^2 \propto (m_u + m_d)$

and $m_{K^0}^2 \propto (m_d + m_s)$, which show the sensitivity of these quantities to the quark masses. In practice one uses higher order ChPT (or other fit functions) to extrapolate or interpolate the lattice results so as to match the desired ratios, correcting for the (small) effects of isospin breaking and electromagnetic corrections. Most present calculations need to extrapolate to the physical value of m_ℓ, while simulating directly at or near to the physical value of m_s.

17.1.4.3. *Heavy quark masses:* Heavy quarks (c and b) are usually treated only as valence quarks, with no loop effects included. The errors introduced by this approximation can be estimated to be $\sim \alpha_s(m_c)\Lambda_{\mathrm{QCD}}^2/m_c^2$ and are likely to be small. For high precision, however, dynamical charm quarks may be necessary, and simulations are beginning to include them.

The heavy quark masses can be tuned by setting heavy-heavy or heavy-light meson masses to their experimental values. For the charm quark, for example, one could use the J/ψ or the D_s meson. Consistency between these two determinations provides an important check that the determination of parameters in the heavy quark lattice formulations is being done correctly (see, e.g. Ref. 37).

17.1.5. *Sources of systematic error* :

Lattice results have statistical and systematic errors that must be quantified for any calculation in order for the result to be a useful input to phenomenology. The statistical error is due to the use of Monte Carlo importance sampling to evaluate the path integral (a method discussed below). There are, in addition, a number of systematic errors that are always present to some degree in lattice calculations, although the size of any given error depends on the particular quantity under consideration and the parameters of the ensembles being used. The most common lattice errors are reviewed below.

Although not strictly a systematic error, it is important to note that the presence of long autocorrelations in the sequence of lattice configurations generated by the Monte Carlo method can lead to uncertainty in the estimates of statistical errors. It is known that the global topological charge of the gauge fields decorrelates very slowly with certain algorithms [38]. This issue is particularly important for quantities, like the η' mass, which are sensitive to topology. It is an active area of research.

17.1.5.1. *Continuum limit:* Physical results are obtained in the limit that the lattice spacing a goes to zero. The Symanzik effective theory determines the scaling of lattice artefacts with a. Most lattice calculations use improved actions with leading discretizations errors of $\mathcal{O}(a^2\Lambda^2)$, $\mathcal{O}(\alpha_s a^2\Lambda^2)$, or $\mathcal{O}(\alpha_s a\Lambda)$, where Λ is a typical momentum scale in the system. Knowledge of the scaling of the leading discretization errors allows controlled extrapolation to $a = 0$ when multiple lattice spacings are available, as in current state-of-the-art calculations. Residual errors arise from the exclusion of subleading a dependence from the fits.

For many quantities the typical momentum scale in the system is $\sim \Lambda_{\mathrm{QCD}} \approx 300$ MeV. Discretization errors are expected to be larger for quantities involving larger scales, for example form factors or decays involving particles with momenta larger than Λ_{QCD}.

17.1.5.2. *Infinite volume limit:* LQCD calculations are necessarily carried out in finite space-time boxes, leading to departures of physical quantities (masses, decay constants, etc.) from their measured, infinite volume values. These finite-volume shifts are an important systematic that must be estimated and minimized.

Typical lattices are asymmetric, with N_s points in the three spatial directions and N_t in the (Euclidean) temporal direction. The spatial and temporal sizes in physical units are thus $L_s = aN_s$ and $L_t = aN_t$, respectively. (Anisotropic lattice spacings are also sometimes used, as discussed below in Sec. 1.3.1.) Typically, $L_t \geq 2L_s$, a longer temporal direction being used to allow excited-state contributions to correlators to decay. This means that the dominant impact of using finite volume is from the presence of a finite spatial box.

At present, high-precision LQCD calculations are of quantities involving no more than a single particle in initial and final states. For such quantities, once the volume exceeds about 2 fm (so that the particle is not "squeezed"), the dominant finite-volume effect comes from virtual pions wrapping around the lattice in the spatial directions. This effect is exponentially suppressed as the volume becomes large, roughly as $\sim \exp(-m_\pi L_s)$, and has been estimated using ChPT [39] or other methods [40]. The estimates suggest that finite volume shifts are sub-percent effects when $m_\pi L_s \gtrsim 4$, and most large-scale simulations use lattices satisfying this condition. This becomes challenging as one approaches the physical pion mass, for which $L_s \gtrsim 5$ fm is required. At present, this can only be achieved by using relatively coarse lattices, $a \gtrsim 0.07$ fm.

Finite volume errors are usually determined by repeating the simulations on two or more different volumes (with other parameters fixed). If different volumes are not available, the ChPT estimate can be used, often inflated to account for the fact that the ChPT calculation is truncated at some order.

In the future, LQCD calculations involving more than a single hadron will become increasingly precise. Examples include the calculation of resonance parameters and $K \to \pi\pi$ amplitudes. Finite volume effects are much larger in these cases, with power-law terms (e.g. $1/L_s^3$) in addition to exponential dependence. Indeed, as will be discussed in Sec. 1.2.4., one can use the volume dependence to indirectly extract infinite-volume quantities such as scattering lengths. Doing so, however, requires a set of lattice volumes satisfying $m_\pi L_s \gtrsim 4$ and is thus more challenging than for single-particle quantities.

17.1.5.3. *Chiral extrapolation:* An important source of systematic error in most LQCD calculations is the need to extrapolate in m_u and m_d (or, equivalently, in m_π). To do this, one needs a functional form that is, at least approximately, valid for pion masses ranging from the unphysical values used in simulations down to the physical value. A theoretically favored choice is to use the predictions of SU(3) or SU(2) ChPT. This is a valid description of QCD for $m_q \ll \Lambda_{QCD}$ (or $m_\pi \ll m_\rho$), but the extent to which it applies at larger pion masses is not known *a priori.* This concern is exacerbated in practice since one must truncate the ChPT expressions, typically at one-loop or two-loop order. Experience to date suggests that one-loop expressions are not sufficiently accurate if $m_\pi \gtrsim 400$ MeV [41].

Another choice of fit function is based on the observation that one does not need

to extrapolate to the chiral limit, but only to the physical, non-zero, value of m_π, and thus an analytic description might suffice. In practice, of course, one must truncate the analytic form at low order, and a concern is whether the curvature from known non-analytic terms is adequately reproduced.

Extrapolation errors are estimated by comparing fits based on ChPT to those using analytic fits, or by varying the fit function in some other way, and/or by varying the number of data points included. We also note that, in many calculations, additional input to the chiral extrapolation is obtained from "partially quenched" results in which the valence and sea-quark masses differ [42].

Recently, simulations with physical light quark masses (except that $m_u = m_d = (m_u^{\mathrm{phys}} + m_d^{\mathrm{phys}})/2$) have been undertaken [43], and are now becoming increasingly common [44]. This is a major step forward as it removes the need for chiral extrapolation. As noted above, such simulations require large boxes, and thus very large lattices, and to date the results have been used to compute a limited number of observables. In the future, however, such simulations will play an increasingly important role in the determination of physical quantities.

17.1.5.4.   *Operator matching:* Many of the quantities that LQCD can precisely calculate involve hadronic matrix elements of operators from the electroweak Hamiltonian. Examples include the pion and kaon decay constants, semileptonic form factors and the kaon mixing parameter B_K (the latter defined in Eq. (17.13)). The operators in the lattice matrix elements are defined in the lattice regularization scheme. To be used in tests of the Standard Model, however, they must be matched to the continuum regularization scheme in which the corresponding Wilson coefficients have been calculated. The only case in which such matching is not needed is if the operator is a conserved or partially conserved current. Similar matching is also needed for the conversion of lattice bare quark masses to those in the continuum $\overline{\mathrm{MS}}$ scheme.

Three methods are used to calculate the matching factors: perturbation theory (usually to one- or two-loop order), non-perturbative renormalization (NPR) using Landau-gauge quark and gluon propagators [45], and NPR using gauge-invariant methods based on the Schrödinger functional [46]. The NPR methods replace truncation errors (which can only be approximately estimated) by statistical and systematic errors which can be determined reliably and systematically reduced.

A common issue that arises in many such calculations (e.g. for quark masses and B_K) is that, using NPR, one ends up with operators regularized in a MOM-like (or Schrödinger functional) scheme, rather than the $\overline{\mathrm{MS}}$ scheme mostly used for calculating the Wilson coefficients. To make contact with this scheme requires a purely continuum perturbative matching calculation. The resultant truncation error can, however, be minimized by pushing up the momentum scale at which the matching is done using step-scaling techniques as part of the NPR calculation [47]. It should also be noted that this final step in the conversion to the $\overline{\mathrm{MS}}$ scheme could be avoided if continuum calculations used a MOM-like scheme.

17.2. Methods and status

Once the lattice action is chosen, it is straightforward to define the quantum theory using the path integral formulation. The Euclidean-space partition function is

$$Z = \int [dU] \prod_f [dq_f][d\bar{q}_f] e^{-S_g[U] - \sum_f \bar{q}_f (D[U] + m_f) q_f} \,, \tag{17.4}$$

where link variables are integrated over the SU(3) manifold, q_f and $\bar{q}_f$ are Grassmann (anticommuting) quark and antiquark fields of flavor f, and $D[U]$ is the chosen lattice Dirac operator with m_f the quark mass in lattice units. Integrating out the quark and antiquark fields, one arrives at a form suitable for simulation:

$$Z = \int [dU] e^{-S_g[U]} \prod_f \det(D[U] + m_f) \,. \tag{17.5}$$

The building blocks for calculations are expectation values of multi-local gauge-invariant operators, also known as "correlation functions",

$$\langle \mathcal{O}(U, q, \bar{q}) \rangle = (1/Z) \int [dU] \prod_f [dq_f][d\bar{q}_f] \mathcal{O}(U, q, \bar{q}) e^{-S_g[U] - \sum_f \bar{q}_f (D[U] + m_f) q_f} \,. \tag{17.6}$$

If the operators depend on the (anti-)quark fields q_f and $\bar{q}_f$, then integrating these fields out leads not only to the fermion determinant but also, through Wick's theorem, to a series of quark "propagators", $(D[U] + m_f)^{-1}$, connecting the positions of the fields.

This set-up allows one to choose, by hand, the masses of the quarks in the determinant (the sea quarks) differently from those in the propagators (valence quarks). This is called "partial quenching", and, as noted above, is used by some calculations as a way of obtaining more data points from which to extrapolate both sea and valence quarks to their physical values.

17.2.1. *Monte-Carlo method* :

Since the number of integration variables U is huge ($N_s^3 \times N_t \times 4 \times 9$), direct numerical integration is impractical and one has to use Monte-Carlo techniques. In this method, one generates a Markov chain of gauge configurations (a "configuration" being the set of U's on all links) distributed according to the probability measure $[dU] e^{-S_g[U]} \prod_f \det(D[U] + m_f)$. Once the configurations are generated, expectation values $\langle \mathcal{O}(U, q, \bar{q}) \rangle$ are calculated by averaging over those configurations. In this way the configurations can be used repeatedly for many different calculations, and there are several large collections of ensembles of configurations (with a range of values of a, lattice sizes and quark masses) that are publicly available through the International Lattice Data Grid (ILDG). As the number of the configurations, N, is increased, the error decreases as $1/\sqrt{N}$.

The most challenging part of the generation of gauge configurations is the need to include the fermion determinant. Direct evaluation of the determinant is not feasible,

as it requires $\mathcal{O}((N_s^3 \times N_t)^3)$ computations. Instead, one rewrites it in terms of "pseudofermion" fields ϕ (auxiliary fermion fields with bosonic statistics). For example, for two degenerate quarks one has

$$\det(D[U] + m_f)^2 = \int [d\phi] e^{-\phi^\dagger (D[U] + m_f)^{-2} \phi} . \tag{17.7}$$

By treating the pseudofermions as additional integration variables in the path integral, one obtains a totally bosonic representation. The price one pays is that the pseudofermion effective action is highly non-local since it includes the inverse Dirac operator $(D[U] + m_f)^{-1}$. Thus, the large sparse matrix $(D[U] + m)$ has to be inverted every time one needs an evaluation of the effective action.

Present simulations generate gauge configurations using the Hybrid Monte Carlo (HMC) algorithm [48], or variants thereof. This algorithm combines molecular dynamics (MD) evolution in a fictitious time (which is also discretized) with a Metropolis "accept-reject" step. It makes a global update of the configuration, and is made exact by the Metropolis step. In its original form it can be used only for two degenerate flavors, but extensions (particularly the rational HMC [49]) are available for single flavors. Considerable speed-up of the algorithms has been achieved over the last two decades using a variety of techniques.

All these algorithms spend the bulk of their computational time on the repeated inversion of $(D[U] + m)$ acting on a source (which is required at every step of the MD evolution). Inversions are done using a variety of iterative algorithms, *e.g.* the conjugate gradient algorithm. In this class of algorithms, computational cost is proportional to the condition number of the matrix, which is the ratio of maximum and minimum eigenvalues. For $(D[U] + m)$ the smallest eigenvalue is $\approx m$, so the condition number and cost are inversely proportional to the quark mass. This is a major reason why simulations at the physical quark mass are challenging. Recent algorithmic studies are making progress in significantly reducing this problem.

A practical concern is the inevitable presence of correlations between configurations in the Markov chain. These are characterized by an autocorrelation length in the fictitious MD time. One aims to use configurations separated in MD time by greater than this autocorrelation length. In practice, it is difficult to measure this length accurately, and this leads to some uncertainty in the resulting statistical errors, as well as the possibility of insufficient equilibration.

For most of the applications of LQCD discussed in this review, the cost of generating gauge configurations is larger than that of performing the "measurements" on those configurations. The computational cost of gauge generation grows with the lattice volume, $V_{\text{lat}} = N_s^3 N_t$, as $V_{\text{lat}}^{1+\delta}$. Here $\delta = 1/4$ for the HMC algorithm [50] and can be reduced slightly using modern variants. Such growth with V_{lat} provides a (time-dependent) limit on the largest lattice volumes that can be simulated. At present, the largest lattices being used have $N_s = 96$ and $N_t = 192$. Typically one aims to create an ensemble of $\sim 10^3$ statistically independent configurations at each choice of parameters (a, m_q and V_{lat}). For most physical quantities of interest, this is sufficient to make the resulting statistical errors smaller than or comparable to the systematic errors.

17.2.2. *Two-point functions* :

One can extract properties of stable hadrons using two-point correlation functions, $\langle O_X(x)O_Y^\dagger(0)\rangle$. Here $O_{X,Y}(x)$ are operators that have non-zero overlaps with the hadronic state of interest $|H\rangle$, *i.e.* $\langle 0|O_{X,Y}(x)|H\rangle \neq 0$. One usually Fourier-transforms in the spatial directions and considers correlators as a function of Euclidean time:

$$C_{XY}(t;\vec{p}) = \sum_{\vec{x}}\langle O_X(t,\vec{x})O_Y^\dagger(0)\rangle e^{-i\vec{p}\cdot\vec{x}}. \tag{17.8}$$

(Here and throughout this section all quantities are expressed in dimensionless lattice units, so that, for example, $\vec{p} = a\vec{p}_{\rm phys}$.) By inserting a complete set of states having spatial momentum $\vec{p}$, the two-point function can be written as

$$C_{XY}(t;\vec{p}) = \sum_{i=0}^{\infty}\frac{1}{2E_i(\vec{p})}\langle 0|O_X(0)|H_i(\vec{p})\rangle\langle H_i(\vec{p})|O_Y^\dagger(0)|0\rangle e^{-E_i(\vec{p})t}, \tag{17.9}$$

where the energy of the i-th state $E_i(\vec{p})$ appears as an eigenvalue of the time evolution operator e^{-Ht} in the Euclidean time direction. The factor of $1/[2E_i(\vec{p})]$ is due to the relativistic normalization used for the states. For large enough t, the dominant contribution is that of the lowest energy state $|H_0(\vec{p})\rangle$:

$$C_{XY}(t)\overset{t\to\infty}{\longrightarrow}\frac{1}{2E_0(\vec{p})}\langle 0|O_X(0)|H_0(\vec{p})\rangle\langle H_0(\vec{p})|O_Y^\dagger(0)|0\rangle e^{-E_0(\vec{p})t}. \tag{17.10}$$

One can thus obtain the energy $E_0(\vec{p})$, which equals the hadron mass m_H when $\vec{p} = 0$, and the product of matrix elements $\langle 0|O_X(0)|H_i(\vec{p})\rangle\langle H_i(\vec{p})|O_Y^\dagger(0)|0\rangle$.

This method can be used to determine the masses of all the stable mesons and baryons by making appropriate choices of operators. For example, if one uses the axial current, $O_X = O_Y = A_\mu = \bar{d}\gamma_\mu\gamma_5 u$, then one can determine m_{π^+} from the rate of exponential fall-off, and in addition the decay constant f_π from the coefficient of the exponential. A complication arises for states with high spins ($j \geq 4$ for bosons) because the spatial rotation group on the lattice is a discrete subgroup of the continuum group SO(3). This implies that lattice operators, even when chosen to lie in irreducible representations of the lattice rotation group, have overlap with states that have a number of values of j in the continuum limit [51]. For example $j = 0$ operators can also create mesons with $j = 4$. A method to overcome this problem has recently been introduced [52,53].

The expression given above for the correlator $C_{XY}(t;\vec{p})$ shows how, in principle, one can determine the energies of the excited hadron states having the same quantum numbers as the operators $O_{X,Y}$, by fitting the correlation function to a sum of exponentials. In practice, this usually requires using a large basis of operators and adopting the variational approach such as that of Ref. 54. One can also use an anisotropic lattice in which a_t, the lattice spacing in the time direction, is smaller than its spatial counterpart a_s. This allows better separation of the different exponentials. Using a combination of these and other technical improvements extensive excited-state spectra have recently been obtained [53,55,56](for a recent review, see Ref. 57).

17.2.3.   *Three-point functions* :

Hadronic matrix elements needed to calculate semileptonic form factors and neutral meson mixing amplitudes can be computed from three-point correlation functions. We discuss here, as a representative example, the $D \to K$ amplitude. As in the case of two-point correlation functions one constructs operators O_D and O_K having overlap, respectively, with the D and K mesons. We are interested in calculating the matrix element $\langle K|V_\mu|D\rangle$, with $V_\mu = \bar{c}\gamma_\mu s$ the vector current. To obtain this, we use the three-point correlator

$$C_{KV_\mu D}(t_x, t_y; \vec{p}) = \sum_{\vec{x},\vec{y}} \langle O_K(t_x, \vec{x})V_\mu(0)O_D^\dagger(t_y, \vec{y})\rangle e^{-i\vec{p}\cdot\vec{x}}, \qquad (17.11)$$

and focus on the limit $t_x \to \infty$, $t_y \to -\infty$. In this example we set the D-meson at rest while the kaon carries three-momentum $\vec{p}$. Momentum conservation then implies that the weak operator V_μ inserts three-momentum $-\vec{p}$. Inserting a pair of complete sets of states between each pair of operators, we find

$$C_{KV_\mu D}(t_x, t_y; \vec{p}) = \sum_{i,j} \frac{1}{2m_{D_i} 2E_{K_j}(\vec{p})} e^{-m_{D_i} t_x - E_{K_j}(\vec{p})|t_y|} \quad \times$$

$$\times \langle 0|O_K(t_x, \vec{x})|K_i(\vec{p})\rangle\langle K_i(\vec{p})|V_\mu(0)|D_j(\vec{0})\rangle\langle D_j(\vec{0})|O_D^\dagger(0)|0\rangle. \quad (17.12)$$

The matrix element $\langle K_i(\vec{p})|V_\mu(0)|D_j(\vec{0})\rangle$ can then be extracted, since all other quantities in this expression can be obtained from two-point correlation functions. Typically one is interested in the weak matrix elements of ground states, such as the lightest pseudoscalar mesons. In the limit of large separation between the three operators in Euclidean time, the three-point correlation function yields the weak matrix element of the transition between ground states.

17.2.4.   *Scattering amplitudes and resonances* :

The methods described thus far yield matrix elements involving single, stable particles (where by stable here we mean absolutely stable to strong interaction decays). Most of the particles listed in the Review of Particle Properties are, however, unstable—they are resonances decaying into final states consisting of multiple strongly interacting particles. LQCD simulations cannot directly calculate resonance properties, but methods have been developed to do so indirectly for resonances coupled to two-particle final states in the elastic regime [58].

The difficulty faced by LQCD calculations is that, to obtain resonance properties, or, more generally, scattering phase-shifts, one must calculate multiparticle scattering amplitudes in momentum space and put the external particles on their mass-shells. This requires analytically continuing from Euclidean to Minkowski momenta. Although it is straightforward in LQCD to generalize the methods described above to calculate four- and higher-point correlation functions, one necessarily obtains them at a discrete and finite set of Euclidean momenta. Analytic continuation to $p_E^2 = -m^2$ is then an ill-posed

and numerically unstable problem. The same problem arises for single-particle states, but can be largely overcome by picking out the exponential fall-off of the Euclidean correlator, as described above. With a multi-particle state, however, there is no corresponding trick, except for two particles at threshold [59].

What LQCD can calculate are the energies of the eigenstates of the QCD Hamiltonian in a finite box. The energies of states containing two stable particles, e.g. two pions, clearly depend on the interactions between the particles. It is possible to invert this dependence and, with plausible assumptions, determine the scattering phase-shifts at a discrete set of momenta from a calculation of the two-particle energy levels for a variety of spatial volumes [58]. This is a challenging calculation, but it has recently been carried through in several channels with quark masses approaching physical values. Channels studied include $\pi\pi$ (for $I = 2$, 1 and 0), $K\pi$, KD and DD^*. For recent reviews see Ref. 60. Extensions to nucleon interactions are also being actively studied [61]. The generalization of the formalism to the case of three particles is under active consideration [62].

It is also possible to extend the methodology to calculate electroweak decay amplitudes to two particles below the inelastic threshold, e.g. $\Gamma(K \to \pi\pi)$ [63]. Results for the $\Delta I = 3/2$ amplitude with physical quark masses have been obtained [64], and significant progress made toward a calculation of the $\Delta I = 1/2$ amplitude [65]. Partial extensions of the formalism above the elastic threshold have been worked out, in particular for the case of multiple two-particle channels [66]. An extension to decays with many multiparticle channels, e.g. hadronic B decays, has, however, yet to be formulated.

17.2.5. *Status of LQCD simulations* :

Until the 1990s, most large-scale lattice simulations were limited to the "quenched" approximation, wherein the fermion determinant is omitted from the path integral. While much of the basic methodology was developed in this era, the results obtained had uncontrolled systematic errors and were not suitable for use in placing precision constraints on the Standard Model. During the 1990s, more extensive simulations including the fermion determinant (also known as simulations with "dynamical" fermions) were begun, but with unphysically high light quark masses ($m_\ell \sim 50 - 100$ MeV), such that the extrapolation to the physical light quark masses was a source of large systematic errors [67]. In the last 5-10 years, advances in both algorithms and computers have allowed simulations to reach much smaller quark masses ($m_\ell \sim 10 - 20$ MeV) and even, as noted above, to work at the physical light quark mass. The net effect is that LQCD calculations of selected quantities now have all sources of error controlled and small, such that they can be used effectively in phenomenological analyses.

On a more qualitative level, analytic and numerical results from LQCD have demonstrated that QCD confines color and spontaneously breaks chiral symmetry. Confinement can be seen as a linearly rising potential between heavy quark and anti-quark in the absence of quark loops. Analytically, this can be shown in the strong coupling limit $g_{\text{lat}} \to \infty$ [1]. At weaker couplings there are precise numerical calculations of the potential that clearly show that this behavior persists in the continuum limit [68,69,70].

Chiral symmetry breaking was also demonstrated in the strong coupling limit on the lattice [15,71], and there have been a number of numerical studies showing that this holds also in the continuum limit. The accumulation of low-lying modes of the Dirac operator, which is the analog of Cooper pair condensation in superconductors, has been observed, yielding a determination of the chiral condensate [72,73,74] Many relations among physical quantities that can be derived under the assumption of broken chiral symmetry have been confirmed by a number of lattice groups [75].

17.3.   Physics applications

In this section we describe the main applications of LQCD that are both computation-ally mature and relevant for the determination of particle properties.

A general feature to keep in mind is that, since there are many different choices for lattice actions, all of which lead to the same continuum theory, a crucial test is that results for any given quantity are consistent. In many cases, different lattice calculations are completely independent and often have very different systematic errors. Thus final agreement, if found, is a highly non-trivial check, just as it is for different experimental measurements.

The number, variety and precision of the calculations has progressed to the point that an international "Flavour Lattice Averaging Group" (FLAG) has been formed. The main aims of FLAG include collecting all lattice results of relevance for a variety of phenomenologically interesting quantities and providing averages of those results which pass appropriate quality criteria. The averages attempt to account for possible correlations between results (which can arise, for example, if they use common gauge configurations). The quantities considered are those we discuss in this section, with the exception of the hadron spectrum. FLAG has recently completed their review [75], and we have made extensive use of it in preparing the following summary. We stress that the results we quote below are those obtained using the physical complement of light quarks (i.e. $N_f = 2 + 1$ or $2 + 1 + 1$ simulations).

17.3.1.   *Spectrum* :

The most basic prediction of LQCD is of the hadron spectrum. Once the input parameters are fixed as described in Sec. 17.1.4, the masses or resonance parameters of all other states can be predicted. This includes hadrons composed of light (u, d and s) quarks, as well as heavy-light and heavy-heavy hadrons. It also includes quark-model exotics (e.g. $J^{PC} = 1^{-+}$ mesons) and glueballs. Thus, in principle, LQCD calculations should be able to reproduce many of the experimental results compiled in the Review of Particle Properties. Doing so would test both that the error budgets of LQCD calculations are accurate and that QCD indeed describes the strong interactions in the low-energy domain. The importance of the latter test can hardly be overstated.

What is the status of this fundamental test? As discussed in Sec. 1.2, LQCD calculations are most straightforward for stable, low-lying hadrons. Resonances which can decay into only two particles are more challenging, though substantial progress has been made. First theoretical work on decays to more than two particles has begun, but the methodology is not yet practical. It is also more technically challenging to calculate

masses of flavor singlet states (which can annihilate into purely gluonic intermediate states) than those of flavor non-singlets, although again algorithmic and computational advances have made such calculations accessible in some cases. The present status for light hadrons is that fully controlled results are available for the masses of the octet light baryons, while results with less than complete control are available for the decuplet baryon resonances, the vector meson resonances and the η and η'. There are more extensive results for heavy-light (D and B systems) and heavy-heavy (J/ψ and Υ systems). All present results, which are discussed in the "Quark Model" review, are consistent with experimental values. For a recent extensive review of lattice results see also Ref. 76.

17.3.2. *Decay constants and bag parameters* :

The pseudoscalar decay constants can be determined from two point correlation functions involving the axial-vector current, as discussed in Sec. 17.2.2. The decay constant f_P of a meson P is extracted from the weak matrix element involving the axial-vector current using the relation $\langle 0|A_\mu(x)|P(\vec{p})\rangle = f_P p_\mu \exp(-ip \cdot x)$, where p_μ is the momentum of P and $A_\mu(x)$ is the axial-vector current. For the pion and kaon decay constants, this calculation is by now straightforward. The ratio f_K/f_π is especially important for the extraction of $|V_{us}|/|V_{ud}|$ from experiment, and many of the systematic errors in the lattice calculation cancel or are significantly reduced when forming the ratio [77]. A number of lattice groups have calculated this ratio with precision at the percent level or better; all the results are in good agreement, with sub-percent precision in the world average [78,79,75]. A summary is shown in Fig. 17.1. The most significant advance in the last two years is the addition of a calculation including dynamical charm quarks ("$N_f = 2 + 1 + 1$") [44], the result from which is in complete agreement with the average of results with $N_f = 2 + 1$.

The heavy-light decay constants f_D and f_{D_s} involve a charm valence quark, which can be simulated using various methods, as discussed in Sec. 17.1.3. The most accurate result uses the same HISQ action for the charm quark as for the light quarks, which means that the matching factor for the axial currents of interest are unity. This allows Ref. 83 to quote values for the charm decay constants with 1-1.5% errors. Calculations using alternative quark actions give consistent results, but with larger errors [84,85]. The FLAG averages are $f_D = 209(3)$ MeV, $f_{D_s} = 249(3)$ MeV, $f_{D_s}/f_D = 1.187(12)$.

The bottom meson decay constants f_B and f_{B_s} require a valence b quark. Lattice calculations of these quantities are available using the Fermilab formulation [84], NRQCD [86] or HQET [87] to treat the bottom quark or using an interpolation between results from around m_c to infinite quark mass [88,89]. Results have precisions ranging down to $\sim 2\%$. The FLAG averages are $f_B = 191(4)$ MeV, $f_{B_s} = 228(5)$ MeV, $f_{B_s}/f_B = 1.20(2)$.

The kaon bag parameter B_K is needed to turn the precise measurement of CP-violation in kaon mixing into a constraint on the Standard Model. It is defined by

$$\frac{8}{3}m_K^2 f_K^2 B_K(\mu) = \langle \overline{K}^0|Q_{\Delta S=2}(\mu)|K^0\rangle, \tag{17.13}$$

where m_K is the kaon mass, f_K is the kaon decay constant, $Q_{\Delta S=2} = \overline{s}\gamma_\mu(1-\gamma_5)d\overline{s}\gamma_\mu(1-\gamma_5)d$ is the four-quark operator of the effective electroweak Hamiltonian and μ is the
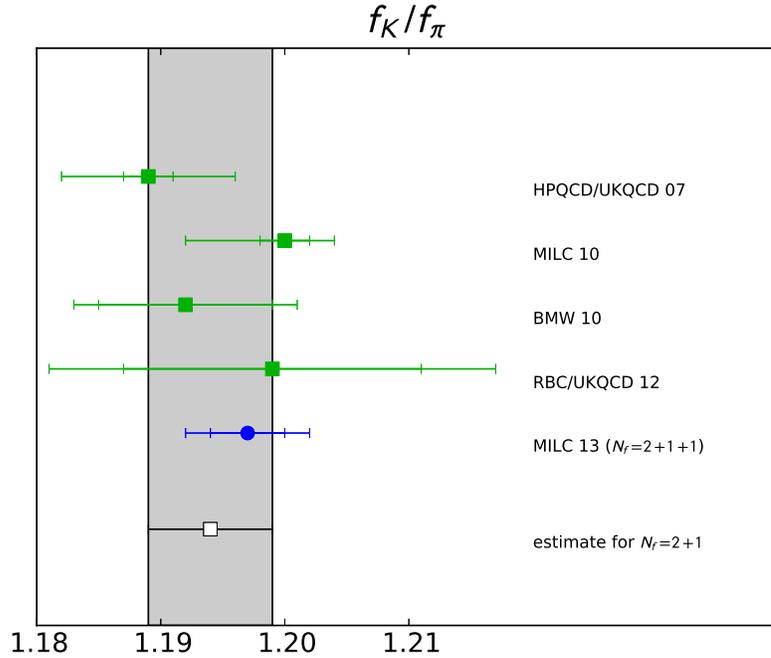
Figure 17.1: Results for f_K/f_π in the isospin limit from simulations with $N_f = 2 + 1$ and $N_f = 2 + 1 + 1$. These are from the HPQCD/UKQCD [37], BMW [80], MILC [81,44], and RBC/UKQCD collaborations [82]. The MILC collaboration results have been shifted upward (by $\sim 0.2\%$, following Ref. 75) since they were originally quoted for $m_u \neq m_d$. The FLAG average of the $N_f = 2 + 1$ results is 1.194 ± 0.005 [75].

renormalization scale. The short distance contribution to the electroweak Hamiltonian can be calculated perturbatively, but the hadronic matrix element parameterized by B_K must be computed using non-perturbative methods. In order to be of use to phenomenology, the renormalization factor of the four-quark operator must be matched to a continuum renormalization scheme, e.g. to $\overline{\text{MS}}$, as described in Sec. 17.1.5.4. Determinations with percent-level precision using different fermion actions are now available with DWF [82], staggered fermions [90], DWF valence on staggered sea quarks [91], twisted mass fermions [92] and Wilson fermions [12]. The results are all consistent, and the FLAG average is $\hat{B}_K = 0.766(10)$.

The bag parameters for B and B_s meson mixing are defined analogously to that for kaon mixing. The B and B_s mesons contain a valence b-quark so that calculations of these quantities must use one of the methods for heavy quarks described above. Calculations have been done using NRQCD [93], the Fermilab formalism [94], the Columbia formalism [95] and twisted-mass fermions [96]. For $f_B\sqrt{B_B}$ and $f_{B_s}\sqrt{B_{B_s}}$ the

averages are dominated by the HPQCD results [93]. The errors ($\sim 7\%$) are dominated by that from operator matching. For the ratio of these two quantities, ξ, the total error ($\sim 5\%$) is somewhat smaller due to cancelations: the dominant errors are due to chiral extrapolation and statistics. The FLAG averages are $f_B\sqrt{B_B} = 216(15)$ MeV, $f_{B_s}\sqrt{B_{B_s}} = 266(18)$ Mev and $\xi = 1.268(63)$.

The results discussed in this section are used in the reviews "The CKM Quark-Mixing Matrix," "V_{ud}, V_{us}, the Cabibbo Angle and CKM Unitarity," and "$B_0 - \bar{B}_0$ Mixing."

17.3.3.   *Form factors* $(K \to \pi\ell\nu,\, D \to K\ell\nu,\, B \to \pi\ell\nu,\, B \to D^{(*)}\ell\nu)$:

Semileptonic decay rates can be used to extract CKM matrix elements once the semileptonic form factors are known from lattice calculations. For example, the matrix element of a pseudoscalar meson P undergoing semileptonic decay to another pseudoscalar meson D is mediated by the vector current, and can be written in terms of form factors as

$$\langle D(p_D)|V_\mu|P(p_P)\rangle = f_+(q^2)(p_D + p_P - \Delta)_\mu + f_0(q^2)\Delta_\mu\,, \qquad (17.14)$$

where $q = p_D - p_P$, $\Delta_\mu = (m_D^2 - m_P^2)q_\mu/q^2$ and V_μ is the quark vector current. The shape of the form factor is typically well determined by experiment, and the value of $f_+(q^2)$ at some reference value of q^2 is needed from the lattice in order to extract CKM matrix elements. Typically $f_+(q^2)$ dominates the decay rate, since the contribution from $f_0(q^2)$ is suppressed when the final state lepton is light.

The form factor $f_+(0)$ for $K \to \pi\ell\nu$ decays is highly constrained by the Ademollo-Gatto theorem [97] and chiral symmetry. Old estimates using chiral perturbation theory combined with quark models quote sub-percent precision [98], though they suffer from some model dependence. The lattice has now matched this precision while also eliminating the model dependence; good agreement with the old estimate is found [99,100,101,102]. The FLAG average is $f_+(0) = 0.967(4)$.

Charm meson semileptonic decays have been calculated by different groups using methods similar to those used for charm decay constants, and results are steadily improving in precision [103,104]. For semileptonic decays involving a bottom quark, one uses HQET or NRQCD to control the discretization errors of the bottom quark. The form factors for the semileptonic decay $B \to \pi\ell\nu$ have been calculated in unquenched lattice QCD by HPQCD [105] and Fermilab/MILC Collaborations [106]. These B semileptonic form factors are difficult to calculate at low q^2, *i.e.* when the mass of the B-meson must be balanced by a large pion momentum, in order to transfer a small momentum to the lepton pair. The low q^2 region has large discretization errors and very large statistical errors, while the high q^2 region is much more accessible to the lattice. For experiment, the opposite is true. To combine lattice and experimental results it has proved helpful to use the z-parameter expansion [107]. This provides a theoretically constrained parameterization of the entire q^2 range, and allows one to obtain $|V_{ub}|$ without model dependence [108,106].

The semileptonic decays $B \to D\ell\nu$ and $B \to D^*\ell\nu$ can be used to extract $|V_{cb}|$ once the corresponding form factors are known. At present only one unquenched calculation exists for the $B \to D^*\ell\nu$ form factor, where the Fermilab formulation of the heavy

quark was adopted [109]. This calculation is done at zero-recoil because that is where the lattice systematic errors are smallest. Calculations of the necessary form factors for both processes at non-zero recoil have been done in the quenched approximation [110] using a step-scaling approach for the heavy quarks. Lattice calculations at non-zero recoil are needed in order to decrease the error associated with the extrapolation of the experimental data to the zero-recoil point.

The results discussed in this section are used in the reviews "The CKM Quark-Mixing Matrix," "V_{ud}, V_{us}, the Cabibbo Angle and CKM Unitarity," and "V_{cb} and V_{ub} CKM Matrix Elements."

17.3.4. *Strong coupling constant* :

As explained in Sec. 17.1.4.1, for a given lattice action, the choice of bare lattice coupling constant, g_{lat}, determines the lattice spacing a. If one then calculates a as described in Sec. 17.1.4.1, one knows the strong coupling constant in the bare lattice scheme at the scale $1/a$, $\alpha_{\text{lat}} = g_{\text{lat}}^2/(4\pi)$. This is not, however, useful for comparing to results for α_s obtained from other inputs, such as deep inelastic scattering or jet shape variables. This is because the latter results give α_s in the $\overline{\text{MS}}$ scheme, which is commonly used in such analyses, and the conversion factor between these two schemes is known to converge extremely poorly in perturbation theory. Instead one must use a method which directly determines α_s on the lattice in a scheme closer to $\overline{\text{MS}}$.

Several such methods have been used, all following a similar strategy. One calculates a short-distance quantity K both perturbatively (K^{PT}) and non-perturbatively (K^{NP}) on the lattice, and requires equality: $K^{\text{NP}} = K^{\text{PT}} = \sum_{i=0}^n c_i \alpha_s^i$. Solving this equation one obtains α_s at a scale related to the quantity being used. Often, α_s thus obtained is not defined in the conventional $\overline{\text{MS}}$ scheme, and one has to convert among the different schemes using perturbation theory. Unlike for the bare lattice scheme, the required conversion factors are reasonably convergent. As a final step, one uses the renormalization group to run the resulting coupling to a canonical scale (such as M_Z).

In the work of the HPQCD collaboration [111], the short-distance quantities are Wilson loops of several sizes and their ratios. These quantities are perturbatively calculated to $\mathcal{O}(\alpha_s^3)$ using the V-scheme defined through the heavy quark potential. The coefficients of even higher orders are estimated using the data at various values of a.

Another choice of short-distance quantities is to use current-current correlators. Appropriate moments of these correlators are ultraviolet finite, and by matching lattice results to the *continuum* perturbative predictions, one can directly extract the $\overline{\text{MS}}$ coupling. The JLQCD collaboration [112] uses this approach with light overlap fermions, while the HPQCD collaboration uses charm-quark correlators and HISQ fermions [113]. Yet another choice of short-distance quantity is the static-quark potential, where the lattice result for the potential is compared to perturbative calculations; this method was used to compute α_s within 2+1 flavor QCD [114]. The ETM Collaboration obtains α_s by a comparison of lattice data for the ghost-gluon coupling with that of perturbation theory [115], providing the first determination of α_s with 2+1+1 flavors of dynamical quarks.

With a definition of α_s given using the Schrödinger functional, one can non-perturbatively control the evolution of α_s to high-energy scales, such as 100 GeV, where the perturbative expansion converges very well. This method developed by the ALPHA collaboration [47] has been applied to 2+1-flavor QCD by the PACS-CS collaboration [116].

The various lattice methods for calculating α_s have significantly different sources of systematic error. Thus the good agreement between the approaches (which can be seen in the "Quantum Chromodynamics" review) provides a strong check on the final result.

17.3.5.   *Quark masses* :

Once the quark mass parameters are tuned in the lattice action, the remaining task is to convert them to those of the conventional definition. Since the quarks do not appear as asymptotic states due to confinement, the pole mass of the quark propagator is not a physical quantity. Instead, one defines the quark mass after subtracting the ultra-violet divergences in some particular way. The conventional choice is again the $\overline{\text{MS}}$ scheme at a canonical scale such as 2 or 3 GeV.

As discussed in Sec. 17.1.5.4, one must convert the lattice bare quark mass to that in the $\overline{\text{MS}}$ scheme. The most common approaches used for doing so are perturbation theory and the NPR method, the latter using an RI/MOM intermediate scheme.

Alternatively, one can use a definition based on the Schrödinger functional, which allows one to evolve the quark mass to a high scale non-perturbatively [117].   In practice, one can reach scales as high as $\sim$100 GeV, at which matching to the $\overline{\text{MS}}$ scheme can be reliably calculated in perturbation theory.

Another approach available for heavy quarks is to match current-current correlators at short distances calculated on the lattice to those obtained in continuum perturbation theory in the $\overline{\text{MS}}$ scheme. This has allowed an accurate determination of $m_c(\overline{\text{MS}})$ [118].

Results are summarized in the review of "Quark Masses".

17.3.6.   *Other applications* :

In this review we have concentrated on applications of LQCD that are relevant to the quantities discussed in the Review of Particle Properties. We have not discussed at all several other applications which are being actively pursued by simulations. Here we list the major such applications. The reader can consult the texts [2,3,4] for further details, as well as the proceedings of recent lattice conferences [119].

LQCD can be used, in principle, to simulate QCD at non-zero temperature and density, and in particular to study how confinement and chiral-symmetry breaking are lost as T and μ (the chemical potential) are increased. This is of relevance to heavy-ion collisions, the early Universe and neutron-star structure. In practice, finite temperature simulations are computationally tractable and relatively mature, while simulations at finite μ suffer from a "sign problem" and are at a rudimentary stage.

Another topic under active investigation is nucleon structure (generalized structure functions) and inter-nucleon interactions.

Finally, we note that there is much recent interest in studying QCD-like theories with more fermions, possibly in other representations of the gauge group. The main interest is to find nearly conformal theories which might be candidates for "walking technicolor" models.

17.4. Outlook

While LQCD calculations have made major strides in the last decade, and are now playing an important role in constraining the Standard Model, there are many calculations that could be done in principle but are not yet mature due to limitations in computational resources. As we move to exascale resources (e.g. 10^{18} floating point operations per second), the list of mature calculations will grow. Examples that we expect to mature in the next few years are results for excited hadrons, including quark-model exotics; $\langle N|\bar{s}s|N \rangle$ and related matrix elements (needed for dark-matter searches); results for moments of structure functions; $K \to \pi\pi$ amplitudes (allowing a prediction of ϵ'/ϵ from the Standard Model); $\bar{K} \leftrightarrow K$ and $\bar{B} \leftrightarrow B$ mixing amplitudes from operators arising in models of new physics (allowing one to constrain these models in a manner complementary to the direct searches at the LHC); hadronic vacuum polarization contributions to muon $g - 2$, the running of α_{EM} and α_s; $\pi \to \gamma\gamma$ and related amplitudes; and perhaps the long-distance contribution to $\overline{K} \leftrightarrow K$ mixing and the light-by-light contribution to muon $g - 2$. There will also be steady improvement in the precision attained for the mature quantities discussed above. As already noted, this will ultimately require simulations with $m_u \neq m_d$ and including electromagnetic effects.

17.5. Acknowledgments

References:
1.   K. G. Wilson, Phys. Rev. **D10**, 2445-2459 (1974).
2.   T. Degrand and C. DeTar, "Lattice Methods for Quantum Chromodynamics," World Scientific (2006).
3.   C. Gattringer and C.B. Lang, "Quantum Chromodynamics on the Lattice: An Introductory Presentation," Springer (2009).
4.   "Modern Pespectives in Lattice QCD: quantum field theory and high performance computing" (Lecture notes of the Les Houches Summer School, Vol. 93) eds. L. Lellouch *et al.*, Oxford Univ. Press. (Aug. 2011).
5.   W. Zimmermann, in "Lectures on Elementary Particles and Quantum Field Theory", ed. S. Deser *et al.*, MIT Press, Cambridge, MA (1971); K. Symanzik, Nucl. Phys. **B226**, 187 (1983); Nucl. Phys. **B226**, 205 (1983).
6.   M. Lüscher and P. Weisz, Commun. Math. Phys. **97**, 59 (1985).
7.   Y. Iwasaki, UT-HEP-118.
8.   H. B. Nielsen and M. Ninomiya, Phys. Lett. **B105**, 219 (1981).
9.   B. Sheikholeslami and R. Wohlert, Nucl. Phys. B **259**, 572 (1985).

10. K. Jansen *et al.*, Phys. Lett. **B372**, 275-282 (1996).

11. M. Lüscher, JHEP **0305**, 052 (2003); Comput. Phys. Commun. 156, 209 (2004) and 165, 199 (2005); M. Hasenbusch, Phys. Lett. **B519**, 177 (2001); C. Urbach *et al.*, Comput. Phys. Commun. 174, 87 (2006).

12. S. Durr *et al.*, Phys. Lett. B **705**, 477 (2011).

13. R. Frezzotti *et al.* [Alpha Collab.], JHEP **0108**, 058 (2001).

14. R. Frezzotti and G. C. Rossi, JHEP **0408**, 007 (2004).

15. L. Susskind, Phys. Rev. D **16**, 3031 (1977).

16. M. Golterman, PoS **CONFINEMENT8**, 014 (2008).

17. C. Bernard, Phys. Rev. D **73**, 114503 (2006); S. R. Sharpe, PoS LAT **2006**, 022 (2006).

18. G. P. Lepage, Phys. Rev. D **59**, 074502 (1999).

19. E. Follana *et al.* [HPQCD and UKQCD Collabs.], Phys. Rev. D **75**, 054502 (2007).

20. P. H. Ginsparg and K. G. Wilson, Phys. Rev. D **25**, 2649 (1982).

21. P. Hasenfratz, V. Laliena, and F. Niedermayer, Phys. Lett. B **427**, 125 (1998).

22. M. Lüscher, Phys. Lett. B **428**, 342 (1998).

23. D. B. Kaplan, Phys. Lett. B **288**, 342 (1992); Y. Shamir, Nucl. Phys. B **406**, 90 (1993); Nucl. Phys. B **417**, 167 (1994).

24. H. Neuberger, Phys. Lett. B **417**, 141 (1998); Phys. Lett. B **427**, 353 (1998).

25. A. Borici, `hep-lat/9912040`; A. D. Kennedy, `hep-lat/0607038`.

26. E. Shintani *et al.* [JLQCD Collab.], Phys. Rev. Lett. **101**, 242001 (2008).

27. A. Bazavov *et al.* [MILC Collab.], Phys. Rev. D **87**, 054505 (2013).

28. R. Baron *et al.* [ETM Collab.], JHEP **1006**, 111 (2010).

29. E. Eichten and B. R. Hill, Phys. Lett. B **234**, 511 (1990).

30. J. Heitger and R. Sommer [ALPHA Collab.], JHEP **0402**, 022 (2004); B. Blossier *et al.* [ALPHA Collab.], JHEP **1012**, 039 (2010).

31. B. A. Thacker and G. P. Lepage, Phys. Rev. D **43**, 196 (1991); G. P. Lepage *et al.*, Phys. Rev. D **46**, 4052 (1992).

32. A. X. El-Khadra *et al.,* Phys. Rev. D **55**, 3933 (1997).

33. S. Aoki *et al.*, Prog. Theor. Phys. **109**, 383 (2003).

34. N. H. Christ *et al.*, Phys. Rev. D **76**, 074505 (2007).

35. Y. Aoki *et al.* [RBC and UKQCD Collabs.], Phys. Rev. D **86**, 116003 (2012).

36. For lecture notes on applications of Chiral Perturbation Theory to lattice QCD, see S. R. Sharpe, `arXiv:hep-lat/0607016` and M. Golterman in Ref. [4].

37. E. Follana *et al.* [HPQCD and UKQCD Collabs.], Phys. Rev. Lett. **100**, 062002 (2008); C. T. H. Davies *et al.* [HPQCD Collab.] Phys. Rev. **D82**, 114504 (2010).

38. M. Lüscher, PoS LATTICE **2010**, 015 (2010); S. Schaefer *et al.* [ALPHA Collab.], Nucl. Phys. B **845**, 93 (2011).

39. G. Colangelo *et al.*, Nucl. Phys. **B721**, 136-174 (2005).

40. M. Lüscher, Commun. Math. Phys. **104**, 177 (1986).

41. J. Noaki *et al.* [JLQCD and TWQCD Collabs.], Phys. Rev. Lett. **101**, 202004 (2008).

42. C. W. Bernard and M. F. L. Golterman, Phys. Rev. **D49**, 486-494 (1994); S. R. Sharpe, Phys. Rev. **D56**, 7052 (1997); S. R. Sharpe and N. Shoresh, Phys. Rev. **D62**, 094503 (2000).

43. S. Aoki *et al.* [PACS-CS Collab.], Phys. Rev. D **81**, 074503 (2010); S. Durr *et al.*, Phys. Lett. B **701**, 265 (2011).

44. A. Bazavov *et al.* [MILC Collab.], Phys. Rev. Lett. **110**, 172003 (2013).

45. G. Martinelli *et al.*, Nucl. Phys. B **445**, 81 (1995).

46. M. Lüscher *et al.*, Nucl. Phys. **B384**, 168 (1992).

47. M. Lüscher *et al.*, Nucl. Phys. B **413**, 481 (1994); M. Della Morte *et al.*, [ALPHA Collab.], Nucl. Phys. B **713**, 378 (2005).

48. S. Duane *et al.*, Phys. Lett. B **195**, 216 (1987).

49. M. A. Clark and A. D. Kennedy, Phys. Rev. Lett. **98**, 051601 (2007).

50. M. Creutz, Phys. Rev. **D38**, 1228 (1988); R. Gupta *et al.*, Phys. Rev. **D38**, 1278 (1988).

51. J. E. Mandula *et al.*, Nucl. Phys. **B228**, 91 (1983); J. E. Mandula and E. Shpiz, Nucl. Phys. **B232**, 180 (1984).

52. H. B. Meyer and M. J. Teper, Nucl. Phys. B658, 113 (2003).

53. J. J. Dudek *et al.*, Phys. Rev. **D82**, 034508 (2010); J. J. Dudek *et al.*, Phys. Rev. **D83**, 111502 (2011); R. G. Edwards *et al.*, Phys. Rev. D **84**, 074508 (2011).

54. M. Lüscher and U. Wolff, Nucl. Phys. **B339**, 222 (1990).

55. G. P. Engel *et al.* [Bern-Graz-Regensburg Collab.], Phys. Rev. **D82**, 034505 (2010).

56. M. S. Mahbub *et al.*, `arXiv:1310.6803` [`hep-lat`].

57. D. Mohler, PoS LATTICE **2012**, 003 (2012).

58. M. Lüscher, Commun. Math. Phys. **105**, 153 (1986); Nucl. Phys. **B354**, 531 (1991) and **B364**, 237 (1991).

59. L. Maiani and M. Testa, Phys. Lett. **B245**, 585 (1990).

60. D. Mohler, PoS LATTICE **2012**, 003 (2012); S. Prelovsek *et al.*, `arXiv:1304.2143` [`hep-ph`].

61. S. R. Beane *et al.*, Int. J. Mod. Phys. **E17**, 1157-1218 (2008); M. J. Savage, Prog. Part. Nucl. Phys. **67**, 140 (2012).

62. K. Polejaeva and A. Rusetsky, Eur. Phys. J. A **48**, 67 (2012); R. A. Briceno and Z. Davoudi, Phys. Rev. D **87**, 094507 (2013).

63. L. Lellouch and M. Lüscher, Commun. Math. Phys. **219**, 31 (2001).

64. T. Blum *et al.*, Phys. Rev. Lett. **108**, 141601 (2012); Phys. Rev. D **86**, 074513 (2012).

65. P. A. Boyle *et al.* [RBC and UKQCD Collabs.], Phys. Rev. Lett. **110**, 152001 (2013).

66. V. Bernard *et al.*, JHEP **1101**, 019 (2011); M. Doring *et al.*, Eur. Phys. J. A **47**, 139 (2011); M. T. Hansen and S. R. Sharpe, Phys. Rev. D **86**, 016007 (2012); R. A. Briceno and Z. Davoudi, `arXiv:1204.1110` [`hep-lat`].

67. C. Bernard *et al.*, Nucl. Phys. Proc. Suppl. **119**, 170 (2003).

68. S. Perantonis and C. Michael, Nucl. Phys. B **347**, 854 (1990).

69. G. S. Bali and K. Schilling, Phys. Rev. D **46**, 2636 (1992).

70. S. Necco and R. Sommer, Nucl. Phys. B **622**, 328 (2002).

71. J. M. Blairon *et al.*, Nucl. Phys. **B180**, 439 (1981).
72. H. Fukaya *et al.* [JLQCD Collab.], Phys. Rev. Lett. **104**, 122002 (2010); H. Fukaya *et al.* [JLQCD and TWQCD Collabs.], Phys. Rev. **D83**, 074501 (2011).
73. L. Giusti and M. Luscher, JHEP **0903**, 013 (2009).
74. K. Cichy, E. Garcia-Ramos, and K. Jansen, JHEP **1310**, 175 (2013) arXiv:1303.1954 [hep-lat].
75. S. Aoki, *et al.*, arXiv:1310.8555 [hep-lat]; itpwiki.unibe.ch/flag/index.php/.
76. Z. Fodor and C. Hoelbling, Rev. Mod. Phys. **84**, 449 (2012).
77. W. Marciano, Phys. Rev. Lett. 93, 231803 (2004).
78. J. Laiho *et al.*, Phys. Rev. **D81**, 034503 (2010).
79. G. Colangelo *et al.*, Eur. Phys. J. **C71**, 1695 (2011).
80. S. Durr *et al.*, Phys. Rev. **D81**, 054507 (2010).
81. A. Bazavov *et al.* [MILC Collab.], PoS **LATTICE2010**, 074 (2010).
82. R. Arthur *et al.* [RBC and UKQCD Collabs.], Phys. Rev. D **87**, 094514 (2013).
83. C. T. H. Davies *et al.* Phys. Rev. D **82**, 114504 (2010); H. Na *et al.*, Phys. Rev. D **86**, 054510 (2012).
84. A. Bazavov *et al.* [FNAL/MILC Collab.], Phys. Rev. D **85**, 114506 (2012).
85. P. Dimopoulos *et al.* [ETM Collab.], JHEP **1201**, 046 (2012).
86. F. Bernardoni *et al.*, PoS LATTICE **2012**, 273 (2012).
87. H. Na *et al.*, Phys. Rev. D **86**, 034506 (2012).
88. C. McNeile *et al.*, Phys. Rev. D **85**, 031503 (2012).
89. N. Carrasco *et al.*, PoS LATTICE **2012**, 104 (2012).
90. T. Bae *et al.* [SWME Collab.], Phys. Rev. Lett. **109**, 041601 (2012).
91. J. Laiho and R. S. Van de Water, PoS LATTICE **2011**, 293 (2011).
92. M. Constantinou *et al.* [ETM Collab.], Phys. Rev. **D83**, 014505 (2011).
93. E. Gamiz *et al.* [HPQCD Collab.], Phys. Rev. **D80**, 014503 (2009).
94. C. M. Bouchard *et al.*, PoS LATTICE **2011**, 274 (2011).
95. C. Albertus *et al.*, Phys. Rev. D **82**, 014505 (2010).
96. N. Carrasco *et al.* [ETM Collab.], PoS LATTICE **2012**, 105 (2012).
97. M. Ademollo and R. Gatto, Phys. Rev. Lett. **13**, 264-265 (1964).
98. H. Leutwyler and M. Roos, Z. Phys. **C25**, 91 (1984).
99. P. A. Boyle *et al.*, Eur. Phys. J. **C69**, 159-167 (2010).
100. V. Lubicz *et al.* [ETM Collab.], Phys. Rev. **D80**, 111502 (2009); PoS LATTICE **2010**, 316 (2010).
101. A. Bazavov *et al.* [FNAL/MILC Collabs.] Phys. Rev. D **87**, 073012 (2013).
102. T. Kaneko *et al.* [JLQCD Collab.], PoS LATTICE **2012**, 111 (2012).
103. H. Na *et al.* [HPQCD Collab.], Phys. Rev. D **84**, 114505 (2011).
104. H. Na *et al.* [HPQCD Collab.], Phys. Rev. **D82**, 114506 (2010).
105. E. Dalgic *et al.* [HPQCD Collab.], Phys. Rev. **D73**, 074502 (2006).
106. J. A. Bailey *et al.*, Phys. Rev. **D79**, 054507 (2009).
107. C. Bourrely *et al.*, Nucl. Phys. **B189**, 157 (1981); C. G. Boyd *et al.*, Phys. Rev. Lett. **74**, 4603 (1995); T. Becher and R. J. Hill, Phys. Lett. **B633**, 61 (2006); C. Bourrely *et al.*, Phys. Rev. **D79**, 013008 (2009).

108. M. C. Arnesen *et al.*, Phys. Rev. Lett. **95**, 071802 (2005).
109. C. Bernard *et al,*, Phys. Rev. **D79**, 014506 (2009); J. A. Bailey *et al.* [Fermilab Lattice and MILC Collabs.], PoS **LATTICE2010**, 311 (2010).
110. G. M. de Divitiis *et al.* Phys. Lett. **B655**, 45 (2007); Nucl. Phys. **B807**, 373 (2009).
111. C. T. H. Davies *et al.* [HPQCD Collab.], Phys. Rev. D **78**, 114507 (2008).
112. E. Shintani *et al.*, Phys. Rev. D **82**, 074505 (2010).
113. C. McNeile *et al.*, [HPQCD Collab.], Phys. Rev. D **82**, 034512 (2010).
114. A. Bazavov *el al.* Phys. Rev. D **86**, 114031 (2012).
115. B. Blossier *et al.* Phys. Rev. D **85**, 034503 (2012); Phys. Rev. Lett. **108**, 262002 (2012).
116. S. Aoki *et al.* [PACS-CS Collab.], JHEP **0910**, 053 (2009).
117. S. Capitani *et al.* [ALPHA Collab.], Nucl. Phys. B **544**, 669 (1999).
118. I. Allison *et al.* [HPQCD Collab.], Phys. Rev. **D78**, 054513 (2008); C. McNeile *et al.* [HPQCD Collab.], Phys. Rev. D **82**, 034512 (2010).
119. D. Leinweber *et al.* (ed.), PoS Lattice **2012** (2012).